A Journal of the Gesellschaft Deutscher Chemiker

Angewandte International Edition GDCh Chemie

www.angewandte.org

Accepted Article

Title: Stabilizing Perovskite Precursor by Synergy of Functional Groups for NiOx-Based Inverted Solar Cells with 23.5% Efficiency

Authors: Mengjia Li, Haiyun Li, Qixin Zhuang, Dongmei He, Baibai Liu, Cong Chen, Boxue Zhang, Thierry Pauporté, Zhigang Zang, and Jiangzhao Chen

To be cited as: *Angew. Chem. Int. Ed.* **2022**, e202206914

Link to VoR: https://doi.org/10.1002/anie.202206914

WILEY-VCH

10.1002/anie.202206914

Stabilizing Perovskite Precursor by Synergy of Functional Groups for NiO_x-Based Inverted Solar Cells with 23.5% Efficiency

Mengjia Li[1#], *Haiyun Li*[2#], *Qixin Zhuang*[2#], *Dongmei He*[2], *Baibai Liu*[2], *Cong Chen*[1,4*], *Boxue Zhang*[3], *Thierry Pauporté*[3], *Zhigang Zang*[2*], *and Jiangzhao Chen*[2*]

[1]State Key Laboratory of Reliability and Intelligence of Electrical Equipment, School of Material Science and Engineering, Hebei University of Technology, Dingzigu Road 1, Tianjin 300130, People' s Republic of China.

[2]Key Laboratory of Optoelectronic Technology & Systems (Ministry of Education), College of Optoelectronic Engineering, Chongqing University, Chongqing 400044, China

[3]Chimie ParisTech, PSL Research University, CNRS, Institut de Recherche de Chimie Paris (IRCP), UMR8247, 11 rue P. et M. Curie, F-75005 Paris, France

[4]Macao Institute of Materials Science and Engineering (MIMSE), Macau University of Science and Technology, Taipa, Macau SAR, 999078 China

[#]These authors contributed equally to this work.

[*]Corresponding authors. E-mail: chencong@hebut.edu.cn, zangzg@cqu.edu.cn, jiangzhaochen@cqu.edu.cn

10.1002/anie.202206914

Abstract

Perovskite solar cells suffer from poor reproducibility due to the degradation of perovskite precursor solution. Herein, we report an effective precursor stabilization strategy *via* incorporating 3-hydrazinobenzoic acid (3-HBA) containing carboxyl (-COOH) and hydrazine (-$NHNH_2$) functional groups stabilizer. The oxidation of I^-, deprotonation of organic cations and amine-cation reaction are main causes of the degradation of mixed organic cation perovskite precursor solution. The -$NHNH_2$ can reduce I_2 defects back to I^- and thus suppress the oxidation of I^-, while the H^+ generated by -COOH can inhibit the deprotonation of organic cations and subsequent amine-cation reaction. The above degradation reactions are simultaneously inhibited by the synergy of functional groups. The inverted device achieves an efficiency of 23.5% (certified efficiency of 23.3%) with excellent operational stability, retaining 94% of the initial efficiency after maximum power point tracking for 601 hours.

Keywords: perovskite precursor solution, degradation, defect passivation, functional groups, perovskite solar cells

10.1002/anie.202206914

Introduction

In recent years, organic-inorganic hybrid metal halide perovskite materials have aroused the wide attention of the community and industry due to the advantages of low cost, adjustable band gap, solution processing, high molar extinction coefficient, low exciton binding energy, and high carrier mobility.[1-6] To date, high-efficiency solution-processed metal halide perovskite solar cells (PSCs) have been reported with a fascinating certified power conversion efficiency (PCE) as high as 25.7%.[7] Although high certified PCE has been obtained, poor reproducibility still poses a serious challenge for the commercial application of perovskite photovoltaic deployment. The whole community has been perplexed by the problem that it is difficult to reproduce device performance for different research groups or for the same person from batch to batch. It has been widely reported that the instability of the state of perovskite precursor solution should be primarily responsible for poor reproducibility.[8-10] The precursor solution aging time would dramatically affect the state of perovskite precursor solution (e.g., colloidal size distribution, intermediate phase, type and content of chemical components), which affects the morphology, grain size, crystallinity, phase purity, trap state density, and accordingly affects final device performance and reproducibility.[11-14] The state of perovskite precursor solution is mainly affected by colloidal particle structure change caused by solute-solvent coordination, oxidation of iodide ions, deprotonation of organic cations and organic amine-organic cation reaction.[15] The previous report shows that the colloidal particle structure change caused by solute-solvent coordination is reversible, which can be controlled by tuning pH.[16] However, how to effectively suppress the oxidation of iodide ions, deprotonation of organic cations and organic amine-organic cation reaction is still a huge challenge. As the aging time increases, the degradation of the chemical compositions in precursor solution would lead to a deviation from the ideal stoichiometric ratio, which results in a significant device performance difference.[17, 18] To address the above issues, there is an urgent need to develop additives to stabilize precursor solution to maintain an accurate stoichiometric ratio

10.1002/anie.202206914

between chemical components, which is crucially important for the fabrication of reproducible, efficient and stable PSCs.

As we mentioned above, the oxidation of iodide ions would lead to instability of perovskite precursor solution. It is well known that iodides (I^-) in metal halide perovskite precursors are readily oxidized into iodine (I_2) during aging. On the one hand, the consumption of I^- ions would make the chemical component ratio in the precursor solution deviate from the ideal stoichiometric ratio. On the other hand, the generated I_2 would serve as carrier nonradiative recombination centers in subsequently prepared perovskite films and remarkably deteriorate the photovoltaic performance of perovskite devices. To overcome the challenge of the oxidation of iodides, some effective strategies have been proposed. For example, Zhang et al. found that adding hypophosphorous acid into perovskite precursor solution can improve film quality via reducing the oxidized I_2 back into I^-.[19] Wang et al. developed a Eu^{3+}–Eu^{2+} redox shuttle to oxidize Pb^0 and reduce I_2, respectively.[20] Chen et al. reported that adding benzylhydrazine hydrochloride into degraded precursor solution can effectively reduce the detrimental I_2 back to I^-.[8] It is worth noting that our group previously developed a multifunctional additive molecule 4F-PHCl with a reductive hydrazine functional group which can effectively reduce the I_2 defects back into I^- and thus improve photovoltaic performance.[21] The above results indicate that reductant molecules and ions are very effective in healing iodine defects through reducing them back to iodide. Nevertheless, the function of the reported additive molecules is relatively simple, which can only inhibit the oxidation of iodide ions but cannot inhibit the deprotonation of organic cations and the addition and elimination reaction between organic amine and organic cation. In view of this, the development of additive molecules that can simultaneously inhibit the above three reactions is particularly important for completely suppressing the degradation of precursor solution, which is key to achieve long-term stability of perovskite precursor solution.

In addition to the oxidation of I^- ions, the degradation of perovskite precursor

10.1002/anie.202206914

solution containing formamidinium (FA^+) and methylammonium (MA^+) can also be triggered by the deprotonation of organic ammonium cation and following addition-elimination reaction.[18] $FAPbI_3$ possesses the narrowest bandgap of 1.45-1.52 eV among all known lead-based metal halide perovskites and has the greatest potential in achieving practical efficiency approaching Shockley-Queisser limit efficiency.[22] Due to the slightly overlarge tolerance factor resulting from the overlarge ionic radius of FA^+ cation, however, black phase (α-phase) $FAPbI_3$ easily transforms into yellow phase (δ-phase).[22] To stabilize α-phase, a small amount of MA^+ cations with smaller ionic radius than FA^+ are usually employed to partially substitute FA^+ cations in $FAPbI_3$. Presently, most of the state-of-the-art PSCs with efficiencies exceeding 24% are fabricated via using mixed-organic-cation MA^+/FA^+-based perovskites as absorbers.[23] Nevertheless, MA^+/FA^+-based perovskite precursor solution has been revealed to be unstable due to not only the oxidation of I^- ions but also the deprotonation reaction of organic ammonium cation and following addition-elimination reaction.[24] Pang et al reported that volatile methylamine (MA) produced by the deprotonation of MA^+ can react with FAI to form *N*-methyl FAI (MFAI).[9] Subsequently, generated MFAI further reacts with MA to form *N*, *N′*-dimethyl FAI (DMFAI). Colella et al. further confirmed the above degradation route by the amine-cation reaction of MA-FA^+ via powerful nuclear magnetic resonance (NMR) spectroscopy.[18] Recently, Shi et al. also revealed the key role of organoamines generated by deprotonation reaction of organic ammonium cations (MA^+ and FA^+) in the degradation of mixed MA^+/FA^+ perovskite precursor solution.[15] Slightly different from the conclusions obtained by Pang et al.[9] and Colella et al.[18], however, they demonstrated that the main decomposition route of organic cations is amine-cation reaction of FA-MA^+ instead of amine-cation reaction of MA-FA^+. In any case, amine-cation reaction of MA-FA^+ and/or FA-MA^+ followed by the deprotonation reaction of organic ammonium cations has been certified to be easy to occur. The consumption of small-sized MA^+ and the formation of large-sized organic cations (MFA^+, $DMFA^+$ and/or FMA^+) over solution aging time would

10.1002/anie.202206914

increase tolerance factor, which results in the formation of yellow δ-phase and thereby deteriorates film quality and device performance, finally contributing to poor reproducibility.

Since the above degradation reactions markedly affect device performance and reproducibility, some efforts have been devoted to stabilizing precursor solution by suppressing the deprotonation and amine-cation reactions. For instance, Qin et al. introduced ITIC-Th into mixed cations-based perovskite precursor solution to effectively suppress the formation of yellow δ-phase by stabilizing the $[PbI_6]^{4-}$ framework via the coordination bond of Pb with S.[25] Seok et al. incorporated elemental sulfur (S_8) into mixed-cation precursor and demonstrated that S_8 can stabilize precursor solution through inhibiting the deprotonation of MA^+ via amine-sulfur coordination.[26] Pang et al. employed triethyl borate as a stabilizer of mixed-organic-cation perovskite precursor solution and uncovered that the triethyl borate can effectively eliminate the impurity phase by restricting the deprotonation of MAI.[27] Shi et al. effectively suppressed the irreversible degradation route of amine-cation reaction by adding aldehydes into mixed-organic-cation perovskite precursor solution to remove organoamines based on Schiff-base reactions.[28] From the perspective of reaction sequence, organic amine-organic cation reactions can be effectively inhibited as long as deprotonation of organic cations is suppressed. Therefore, it is critical to suppress the deprotonation decomposition reaction of organic cations to thoroughly stabilize perovskite precursor solution. The oxidation of iodide ion, deprotonation of organic cation and reaction of organic amine-organic cation often occur simultaneously in the mixed organic cation precursor. However, the function of presently reported precursor stabilizers is relatively simple, which can only suppress the oxidation of iodide ions, deprotonation of organic cations or irreversible amine-cation reaction. Consequently, it is highly desirable to develop novel additive molecules that can simultaneously inhibit the above three degradation reactions to obtain long-term stable precursor solutions and achieve reliable and reproducible device performance.

10.1002/anie.202206914

PSCs are fabricated as either n-i-p (regular) or p-i-n (inverted) structures. Recently, the inverted PSCs have demonstrated promising PCEs over 24%,[2, 29, 30] which is comparable to that of regular devices. In these works, organic hole transport materials (HTM) were adopted, which still would reduce the thermal and light stability of the corresponding solar cells. In contrast, the inverted PSCs based on nickel oxide (NiO_x) inorganic HTM exhibit enormous advantages regarding thermal and operational stability over organic HTMs. To date, the PCE over 23% was realized for NiO_x-based inverted PSCs.[31, 32] However, the PCE of NiO_x-based inverted PSCs is much lower than that of regular PSCs. The trap-mediated nonradiative recombination resulting from grain boundary (GB) defects is one critical factor impeding the further improvement of the photovoltaic performance of NiO_x-based inverted PSCs.[33, 34] In view of this, it is highly expected to develop multifunctional molecules to both stabilize precursor solution and passivate the defects at GBs for the simultaneous enhancement of efficiency, stability, and reproducibility toward commercial application.

In this work, we develop a precursor stabilization and defect passivation strategy by employing 3-hydrazinobenzoic acid (3-HBA) containing both carboxyl (-COOH) and hydrazine ($-NHNH_2$) functional groups as a versatile additive. It was revealed that the degradation mechanisms of mixed-organic-cation perovskite precursor solution were mainly involved in the oxidation of I^-, the deprotonation of organic cations, and following amine-cation reaction. The $-NHNH_2$ in 3-HBA can reduce I_2 defects back to I^- and thus suppress the oxidation of I^-. At the same time, -COOH in 3-HBA as weak acid can produce hydrogen proton by reversible equilibrium ionization reaction. The formed H^+ can inhibit the deprotonation of organic cations and subsequent amine-cation reaction. The synergistic effect of $-NHNH_2$ and -COOH resulted in the simultaneous suppression of the above degradation reactions. Additionally, the 3-HBA can also play a role in passivating grain boundary defects, reducing trap density, and increasing carrier lifetimes regardless of perovskite composition and device configuration. As a result, the

resulting NiO_x-based inverted PSC delivered an appealing efficiency of 23.5%, which is one of the highest efficiencies ever reported for NiO_x-based inverted PSCs. The modified devices maintained 94% of the initial PCE after tracking at maximum power point for 601 hours.

Results and discussion

3-HBA containing both -COOH and $-NHNH_2$ functional groups (**Figure 1a**) was directly introduced into fresh triple-cation perovskite precursor solution simultaneously containing FA^+ and MA^+ organic cations (**Figure 1b**). For clarification purposes, the perovskite precursor solutions without and with 3-HBA were denoted as control and target solution, respectively. The photographs of perovskite films fabricated from the control and target solutions at different aging times in **Figure 1c** revealed that both perovskite films are very black. The perovskite films from control solutions gradually turn yellow with the increase of aging time and is almost completely yellow upon aging for 75 d. This indicates that precursor solution aging would lead to the formation of non-perovskite phase due to the consumption of small-sized MA^+ and the formation of large-sized MFA^+ and $DMFA^+$, which will be discussed thereinafter. In contrast, the perovskite films from target solutions always maintain black even if aging time is extended to 75 d. It suggests that 3-HBA additive can effectively stabilize perovskite precursor solution and suppress the formation of non-perovskite phase. As shown in **Figure 1d,e**, the absorption intensity of perovskite films from target solutions is maintained regardless of aging time whereas a significant decrease in absorption intensity over aging time is observed for the perovskite films from control solutions, which is well consistent with the color evolution trend of perovskite films in **Figure 1c**. X-ray photoelectron spectroscopy (XPS) measurement of the perovskite films from control and target solutions after aging for 75 d was carried out. As displayed in **Figure 1f,g**, the metallic lead (Pb^0) peaks at 141.35 and 136.49 eV[35] are obviously observed in the control perovskite film while no these peaks in the target perovskite film. This implies that 3-HBA can inhibit the generation of Pb^0 via the coordination between -COOH and

10.1002/anie.202206914

undercoordinated Pb^{2+}. In addition, it also shows that the hydrazine functional group would not reduce the Pb^{2+} to Pb^{0}. It can be seen clearly from C 1s spectra in **Figure S1** that the peak of O-C=O at 288.60 eV appears in the perovskite film from aged target solution, which is indicative of the existence of 3-HBA in the final perovskite film.

Steady-state photoluminescence (SSPL) spectroscopies were collected to evaluate the carrier recombination of the perovskite films from the control and target solutions before and after aging for 75 d, as shown in **Figure 1h and i**. We can see that the perovskite film from the aged control solution exhibits remarkably reduced PL intensity than that from the fresh control solution while similar PL intensity is found for the perovskite films from fresh and aged target solutions. The photograph, UV-vis absorption, and PL results indicate that 3-HBA can effectively stabilize perovskite precursor solution. Interestingly, the PL peak of the perovskite film from the control solution is red-shifted after aging but the same peak position is found for the perovskite films from target solutions before and after aging, which could be owing to the consumption of MA^{+} cations in precursor by deprotonation. This deprotonation process will be confirmed hereinbelow. To investigate the effect of aging time on device performance, we fabricated NiO_x-based inverted PSCs based on the control and target precursor solutions aging for different times (**Figure 1j, k** and **Figure S2**). All photovoltaic parameters of the devices from control solutions reduce significantly as aging time prolongs. In stark contrast, a just slightly reduced all photovoltaic parameters are observed for the devices from the aged target solutions even 75 d as compared to the device from the fresh target solution. The above results indisputably suggest that 3-HBA can efficaciously improve the reproducibility of PSCs by acting as a stabilizer of the precursor solution.

10.1002/anie.202206914

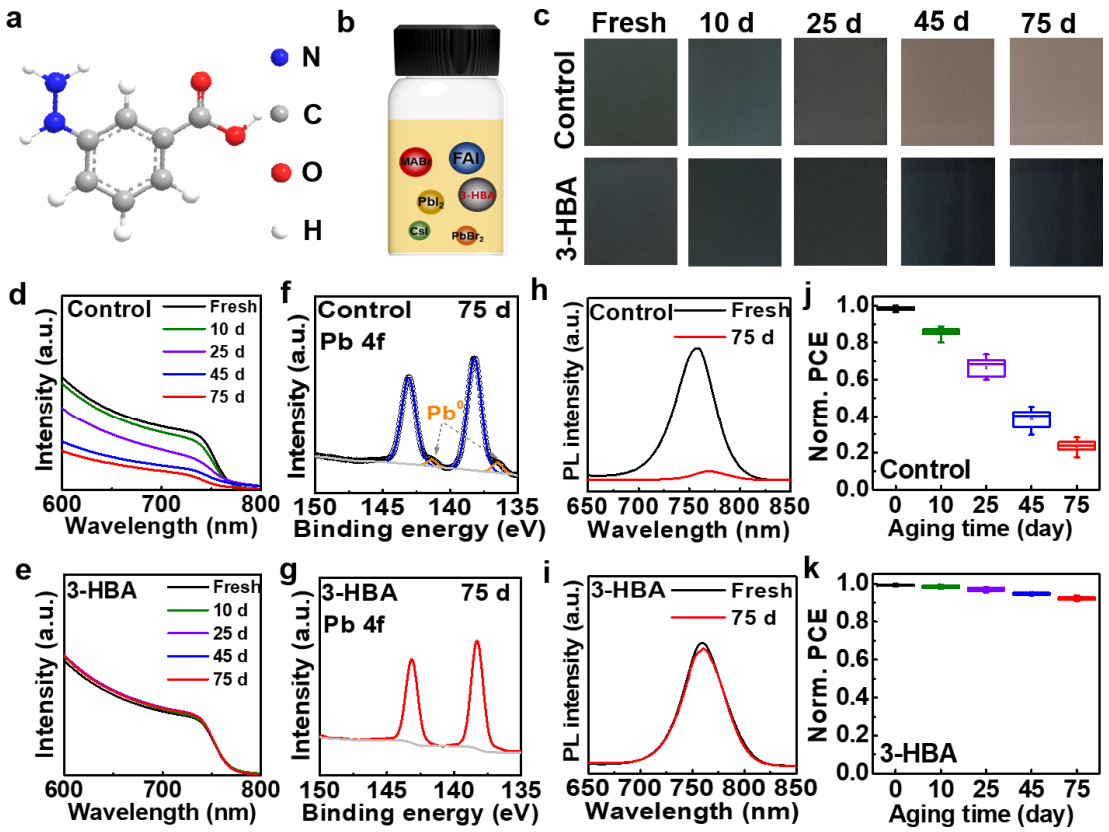

Figure 1. a) Chemical structure of 3-HBA. b) Schematic illustration of perovskite precursor solution incorporating 3-HBA. c) Photographs of the perovskite films prepared by precursor solutions without and with 3-HBA aged for different times. UV-vis absorption spectra of the perovskite films made by precursor solutions d) without and e) with 3-HBA aged for different times. Pb 4f XPS spectra of the perovskite films fabricated from the precursor solutions f) without and g) with 3-HBA aged for 75 d. PL spectra of the perovskite films from the solutions h) without and i) with 3-HBA before and after being aged for 75 d. PCE evolution of the devices fabricated from precursor solutions j) without and k) with 3-HBA aged for different times.

Scanning electron microscopy (SEM) measurement was performed to study the effect of precursor solution aging time on the morphology of perovskite films. As exhibited in **Figure S3**, similar morphology is observed for the perovskite films fabricated from fresh control and target solutions. However, the morphology difference is gradually enlarged as the aging time increases. Up to 25 d, huge

10.1002/anie.202206914

morphology differences can be perceived for control and target films. Until 75 d, the morphology difference is further markedly magnified. We can clearly see that only small pin-holes appear in the target film while huge pin-holes are in the control film. The terrible morphology could be associated with the formation of the impurity phase. The results show that the target precursor solution possesses much more excellent reproducibility than the control solution, which again confirms the stabilization function of 3-HBA for the precursor solution. Subsequently, X-ray diffraction (XRD) patterns were measured to evaluate the effect of aging time on the crystal structure and phases of the perovskite films from the control and target precursor solutions (**Figure 2a and b**). For the films fabricated from the control solution, a main diffraction peak corresponding to the α-phase located at ~14.2° is gradually weakened as the aging time increases. Meanwhile, the diffraction peak at around ~11° due to the formation of δ-phase[9, 28] appears in the perovskite films from aged solutions and peak intensity gradually increases as the aging time extends. As can be seen from enlarged XRD patterns in **Figure 2a**, there is a gradual shift tendency toward lower diffraction angle with the increase of aging time for the peaks of impurity phase as compared to the peak position of pure δ-$FAPbI_3$ (11.74°), which should result from the incorporation of large-sized organic cation (MFA^+ and $DMFA^+$) byproducts into the crystal structure of non-perovskite.[9] In contrast, the introduction of the 3-HBA stabilizer leads to similar intensities of the (110) diffraction peaks due to α-phase for all perovskite films with different aging times (**Figure 2b**). It can be seen from magnified XRD patterns in **Figure 2b** that no impurity δ-phase peak is detected for all perovskite films from target solutions aged for different times. These results suggest that 3-HBA can stabilize mixed-organic-cation perovskite precursor solution by suppressing the formation of δ impurity phase. To clarify the contribution of functional groups in 3-HBA molecules in stabilizing precursor solution, systematic contrast experiments were carried out through adding various additive molecules containing -COOH or $-NHNH_2$ functional groups into precursor solution, including phenylhydrazine (PH), benzoic acid (BA), benzene (C_6H_6), formic acid (HCOOH),

10.1002/anie.202206914

m-methylbenzoic acid (3-MBA) and 3-Aminobenzoic acid (3-ABA). As exhibited in **Figure 2c, d**, α-phase can still be observed until 75 d of aging for the perovskite films from solutions with PH or BA. This indicates that both PH and BA can suppress the formation of δ impurity phase in comparison with the control solution. Nevertheless, PH and BA are much less effective than 3-HBA. A more substantial shift toward a lower angle is found for the diffraction peak of the δ impurity phase in the perovskite films from aged solution with PH as compared to from aged solution with BA. It means that a larger number of large-sized organic cation byproducts is generated in the former film than in the latter film. This proves that -COOH functional group is more effective in suppressing the degradation of organic cations and thus stabilizing precursor solution compared with -$NHNH_2$. It is easily found that benzene does not contribute to stabilizing the solution (**Figure 2e**). We also can find that all additive molecules containing -COOH functional groups including HCOOH, 3-ABA, and 3-MBA have almost the same effect as BA in stabilizing solution. Moreover, the -NH_2 and -CH_3 functional groups in the interposition of the benzoic acid barely work (**Figure 2f-h**). This shows that the hydrazine group plays an indispensable role in stabilizing the solution. It can be concluded that -COOH and -$NHNH_2$ functional groups exhibit synergistic effects in inhibiting the decomposition of organic cations and accordingly the formation of the yellow phase.

10.1002/anie.202206914

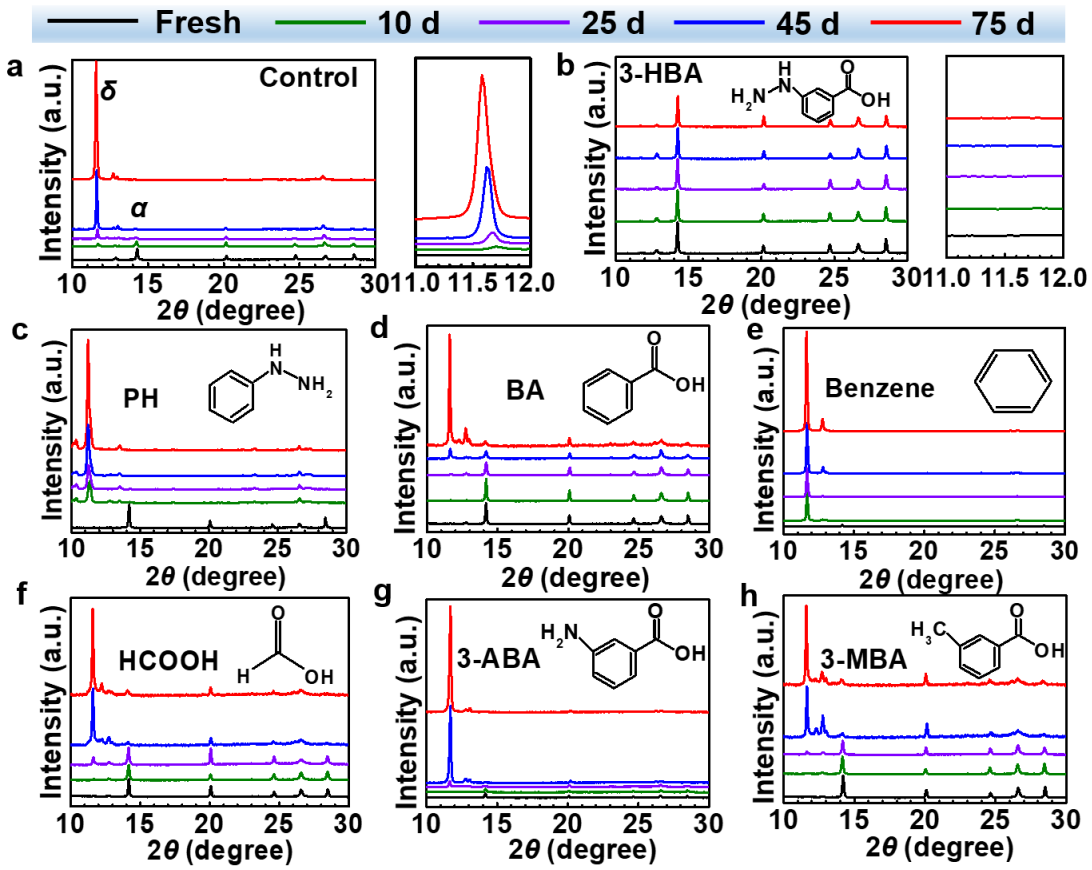

Figure 2. a) control, b) with 3-HBA, c) with PH, d) with BA, e) with C_6H_6, f) with HCOOH, g) with 3-ABA, and h) 3-MBA aged for different times. The illustration shows the chemical structures of the additive molecules.

To further uncover the degradation and inhibition mechanisms by investigating the evolution of reactants and products, we conducted NMR measurement for the control and modified perovskite precursor solutions with 3-HBA and BA aged in the dark at room temperature for different times (**Figure 3a-c**). The deuterium dimethyl sulfoxide (DMSO-d6) was chosen to avoid the interference of the residual signals from dimethylformamide (DMF).[18] We observe the peak signals of MA^+ and FA^+ in all solutions regardless of the introduction of additives. The ^1H signal of methyl (CH_3) in MA^+ is at δ = 2.30 ppm and the ^1H signal of methyne (CH) in FA^+ is at δ = 7.78 ppm.[9, 18] Reduce of MA^+ and FA^+ is attributed to the deprotonation of organic cations, which has been certified by the previous reports.[9, 18, 28] It is worth noting that some new characteristic peaks appear and become stronger and stronger in the control

10.1002/anie.202206914

solutions as the aging time increases (**Figure 3a**). The ^{1}H signal peaks at δ = 2.74 and 7.85 ppm belong to MFA^+ and the ^{1}H signal peak at δ = 2.92 ppm belongs to $DMFA^+$.[9, 18] The formed MA will react with FA^+ to generate MFA^+ by addition-elimination reaction. Generated MFA^+ will further react with another MA by addition-elimination reaction to form $DMFA^+$. For the sake of discussion, we quantified the reactants (including MA^+ and FA^+) and products (including MFA^+ and $DMFA^+$) by integrating the ^{1}H signal peaks (**Figure S4-S18**). The calculation method for the percentage of each composition is given in **Figure S19**. The percentage of left MA^+, left FA^+, generated MFA^+, and generated $DMFA^+$ in precursor solutions without and with additives are plotted as aging time (**Figure 3d-g**). Obviously, the amount of MA^+ and FA^+ is maintained at 100% regardless of aging time for the 3-HBA-containing solution while the amount of MA^+ and FA^+ gradually declines with the prolonging of aging time but reduces much more rapidly for the control solution than the BA-containing solution (**Figure 3d, e**). This indicates that 3-HBA completely suppresses the deprotonation of organic cations and the BA is also effective but much less effective than 3-HBA. It again confirms that -COOH and -$NHNH_2$ play a synergy role in inhibiting the deprotonation of organic cations, which is in good agreement with the conclusion drawn by XRD results. Besides, the deprotonation of MA^+ is much faster compared with that of FA^+, which could be due to the weaker alkalinity of the former than the latter. This also proves that MA-based perovskites are usually less stable with respect to the FA-based perovskites.[36] There is no MFA^+ and $DMFA^+$ in the 3-HBA-containing solution (**Figure 3f, g**), which is reasonable because no MA can be used for the irreversible degradation route of amine-cation reaction since the first step deprotonation reaction of MA^+ is blocked thoroughly. In contrast, we can observe the generation of MFA^+ and $DMFA^+$ in the aged control solution and produced amount is more and more as the aging time extends. However, only MFA^+ can be detected in the aged BA-containing solution and generating rate is much slower for the aged BA-containing solution than the aged control solution. Moreover, no $DMFA^+$ is formed in the aged BA-containing solution. It is easy to understand that

$DMFA^+$ is more difficult to be generated than MFA^+. In short, we can conclude that -COOH and $-NHNH_2$ can synergistically stabilize precursor solution by suppressing the deprotonation of organic cations and thereby subsequent amine-cation reaction. To understand the effect of generated large-sized organic cations on phase stability, we calculated the tolerance factor (τ) by the equation $\tau = \frac{r_A + r_X}{\sqrt{2}(r_B + r_X)}$, where r_A, r_B, and r_X represent the ionic radius of A, B, and X, respectively. The τ is plotted as the substitution ratio of MFA^+ in $FA_{1-x}(MFA)_xPbI_3$ (**Figure 3h**). The pure $FAPbI_3$ has a τ of 0.987 slightly higher than the ideal value, which easily leads to the formation of yellow δ-phase. The τ is enlarged gradually from 0.987 to 1.041 as the substitution ratio increases (**Table S2**). This suggests that doped $FAPbI_3$ perovskite with MFA^+ is more unstable than pure $FAPbI_3$. Consequently, the formation of the yellow phase in precursor solution is not only because of the consumption of MA^+ but also the generation of large-sized cations (MFA^+ and $DMFA^+$). In this work, 3-HBA can suppress the formation of the yellow phase by inhibiting the decomposition of MA^+ and the generation of MFA^+ and $DMFA^+$.

The oxidation of I^- to I_2 is another main degradation route of perovskite precursor solution.[8] We also explored whether the organic functional groups in 3-HBA can effectively suppress the degradation process through measuring the UV-vis absorption spectra of the commercial HI solutions without and with 3-HBA, PH, or BA additive aged for 75 d. It is well known that we can still observe the formation of a large amount of I_2 when we open the bottle of commercial HI solution as presented in **Figure S20a**. This shows that I^- is extremely easy to be oxidized to I_2 even if in the presence of a tiny amount of oxygen. As exhibited in **Figure 3i**, very strong peaks at 365 nm are detected for the control and BA-containing HI solutions, which should be ascribed to the generation of I_2 or I_3^-.[8, 37, 38] This suggests that the BA only containing -COOH can not suppress the oxidation of I^-. In contrast, only a very weak peak is observed in the PH-containing HI solution but this peak can not be detected in the 3-HBA-containing HI solution. This indicates that both PH and 3-HBA

10.1002/anie.202206914

can inhibit the oxidation reaction by reducing I_2 back to I^- but 3-HBA simultaneously containing -$NHNH_2$ and -COOH is slightly more effective than PH only containing -$NHNH_2$. The UV-vis absorption result is consistent with the colour change tendency of HI solutions before and after aging for 75 d (**Figure S20**). Up to now, we can conclude that well-designed 3-HBA can not only suppress the deprotonation of organic cations and the following irreversible degradation route of amine-cation reaction but also inhibit the oxidation of I^-.

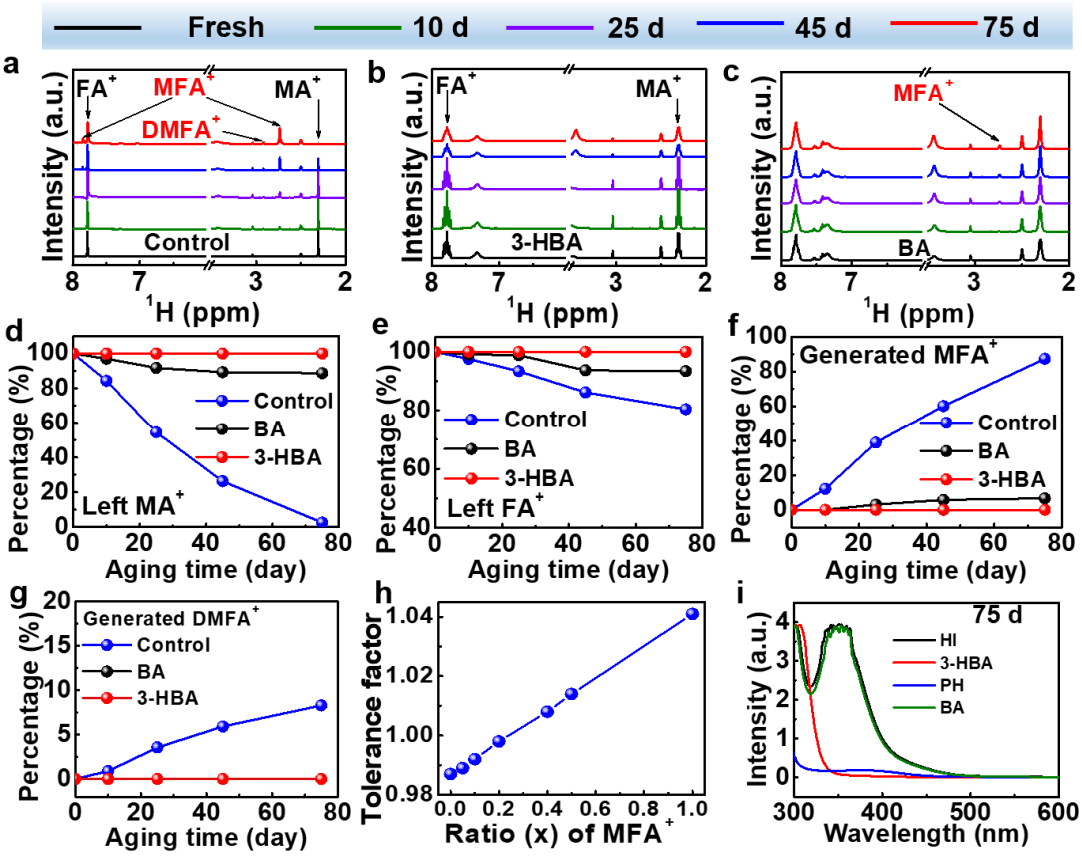

Figure 3. ^{1}H NMR spectra of the perovskite precursor solution of a) control and modified perovskite precursor solutions with b) 3-HBA, and c) with BA aged for different times. Evolution of d) left MA^+, e) left FA^+, f) generated MFA^+, and g) $DMFA^+$ in the control perovskite precursor solution and modified perovskite precursor solutions with 3-HBA and BA aged for different times. h) Tolerance factor of $FA_{1-x}(MFA)_xPbI_3$ perovskite. i) UV-vis absorption spectra of the degraded commercial HI precursor solution without or with 3-HBA, PH, and BA as additives aged for 75 d.

10.1002/anie.202206914

As we discussed above, the degradation of perovskite precursor solution is initially triggered by the deprotonation of organic cations, as shown in reaction (i) in **Figure 4a**. Subsequently, the formed methylamine (MA) would nucleophilically attack the methine carbon of FA^+ and then NH_3 is eliminated, which generates the MFAI product, as presented in reaction (ii).[18] Afterwards, the DMFAI will be produced by the further nucleophilic addition of methylamine to methine carbon of MFA^+ and subsequent elimination of NH_3, as illustrated in reaction (iii).[18] The reaction (iv) shows the deprotonation of FAI. The reactions (i)-(iv) are the main routes of chemical decomposition of mixed FA/MA-based perovskite precursor solution. The above decomposition reactions should be blocked for realizing long-term stable precursor solutions toward reproducible fabrication of efficient and stable PSCs. As displayed in reaction (v), the I^- ions in the solution are oxidized to I_2. It can be found from reaction (vi) that the 3-HBA can ionize to produce protons. In addition, 3-HBA can reduce formed I_2 in reaction (v) to I^- during which H^+ is produced. The generated H^+ ions can inhibit the deprotonation of organic cations and thus the following irreversible amine-cation reaction is effectively suppressed. In brief, 3-HBA can stabilize the precursor solution by suppressing the oxidation of I^-, the deprotonation of organic cations and the following amine-cation reaction. **Figure 4b** schematically illustrates the effect of 3-HBA on the phase stability of perovskite films based on the solutions without and with 3-HBA. The α-$FAPbI_3$ film can be obtained based on the fresh precursor solution due to the presence of enough MA^+. After the precursor is aged, non-perovskite phase is formed because of the consumption of small-sized MA^+ and the generation of large-sized organic cations (MFA^+ and $DMFA^+$). Upon the incorporation of 3-HBA in precursor, the α-$FAPbI_3$ film can still be obtained as the fresh control solution even if the solution is aged. It needs to be stressed that the $-NHNH_2$ can form hydrogen bond with halide ions and the -COOH can coordinate with undercoordinated Pb^{2+}, which results in effective passivation of the defects at GBs of perovskite films. The defect passivation effect will be discussed hereinbelow.

10.1002/anie.202206914

To sum up, the -NHNH$_2$ in 3-HBA can reduce I_2 defects back to I^- and thus suppress the oxidation of I^-. The H^+ which is generated by the -COOH in 3-HBA via reversible equilibrium ionization reaction can inhibit the deprotonation of organic cations and subsequent amine-cation reaction. The degradation reactions are simultaneously inhibited through the synergistic effect of -NHNH$_2$ and -COOH, thereby stabilizing the precursor solution.

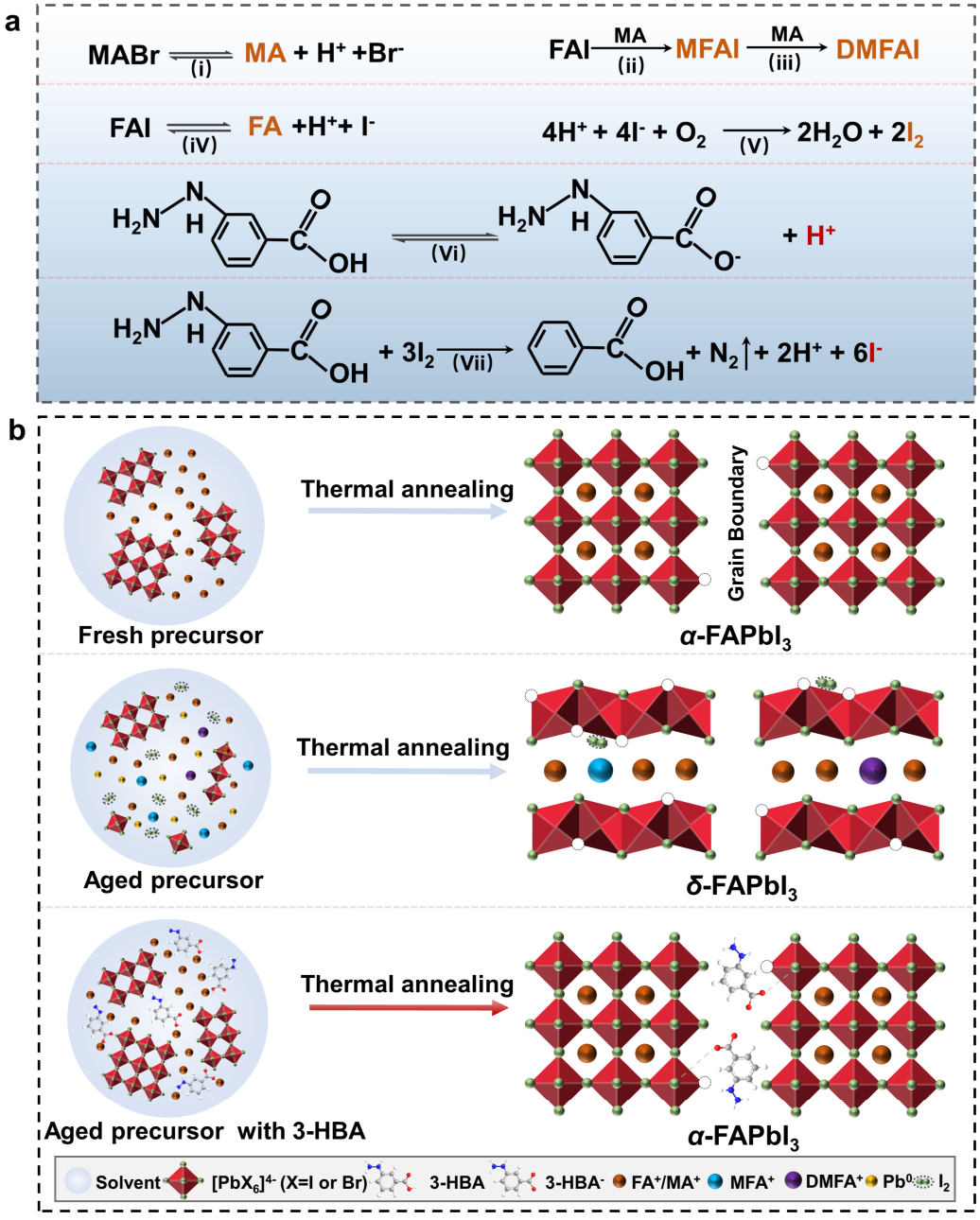

Figure 4. a) Degradation mechanism of mixed-organic-cation perovskite precursor solution and inhibition degradation mechanism by the synergistic effect of -COOH

and -$NHNH_2$ in 3-HBA molecule. Reaction (i) is the deprotonation reaction of MABr. Reaction (ii) is the addition-elimination reaction between MA and FAI. Reaction (iii) is the addition-elimination reaction between MA and MFAI. Reaction (iv) is the deprotonation reaction of FAI. Reaction (v) is the oxidization of I^- by O_2. Reaction (vi) is Equilibrium proton ionization reaction of 3-HBA. Reaction (vii) is the reduction reaction between 3-HBA and I_2. b) Schematic illustration of the suppression of the formation of non-perovskite phase with 3-HBA.

We also can observe the peaks of O=C-O and C-C from 3-HBA in the perovskite film using the fresh solution with 3-HBA (**Figure 5a**), which confirms the existence of 3-HBA in the final perovskite film. As shown in **Figure 5b**, the binding energies of Pb $4f_{5/2}$ and Pb $4f_{7/2}$ are increased from 142.59 eV and 137.73 eV to 142.83 eV and 137.97 eV after the addition of 3-HBA, which is due to coordination interaction between -COOH and undercoordinated Pb^{2+}.[36] From Fourier transform infrared (FTIR) spectra in **Figure 5c**, the stretching vibration peak (1689 cm^{-1}) of the carbonyl (C=O) in 3-HBA is shifted to lower wavenumber (1674 cm^{-1}) upon interaction with PbI_2, which again testifies the strong chemical interaction of 3-HBA with Pb^{2+}, which agrees with the above XPS result. Subsequently, the interaction between 3-HBA with Pb^{2+} is further consolidated by the NMR spectra of 3-HBA and 3-HBA+PbI_2. As shown in **Figure 5d**, the ^1H NMR peak of -COOH in bare 3-HBA (10.23 ppm) is shifted to the lower chemical shift (9.91 ppm) in the 3-HBA+PbI_2 sample. At the same time, it is found that the ^{13}C NMR peak at 167.56 ppm of bare 3-HBA belongs to the carboxyl group, which is shifted to 167.51 ppm after the introduction of PbI_2 (**Figure 5e**). The high-resolution transmission electron microscope (HRTEM) measurement confirms the presence of 3-HBA at GBs of perovskite films (**Figure S21**).

Figure 5f show that the electron trap state density in 3-HBA-modified perovskite film (2.0×10^{15} cm^{-3}) is lower than that in pristine film (6.6×10^{15} cm^{-3}). Meanwhile, **Figure S22** demonstrated that the 3-HBA-modified perovskite film

(2.6×10^{15} cm^{-3}) exhibits reduced hole trap state density than the bare film (3.9×10^{15} cm^{-3}). It suggests that 3-HBA can effectively mitigate nonradiative recombination by passivating the defects at GBs. The effect of 3-HBA passivation on the carrier recombination of perovskite films based on fresh and aged precursor solutions was investigated through measuring the time-resolved photoluminescence (TRPL) spectra (**Figure 5g**). As presented in **Table S3**, the carrier lifetime of the perovskite film from the control solution aged for 75 d (51.77 ns) is reduced by 57% compared with that of the perovskite film fabricated from the fresh control solution (119.15 ns). However, the carrier lifetime is decreased from 809.97 ns of the perovskite film from the fresh target solution to 635.33 ns of the perovskite film from the aged target solution for 75 d, which corresponds to a reduction of 16%. On the one hand, for the fresh solution, the carrier lifetime is significantly increased from 119.15 ns to 608.64 ns after the incorporation of 3-HBA. This proves the effective passivation of 3-HBA for the defects at GBs, which is consistent with reduced defect density. On the other hand, the degradation rate of the control solution is much faster than that of the target solution because 3-HBA can not only suppress the oxidation of I^- but also can inhibit the deprotonation of organic cations and thus addition-elimination reaction.

The much increased average local surface potentials from -109.01 mV to +245.19 mV indicats that the 3-HBA modification has a positive effect on the band edge of grain boundaries and can promote carrier transport in perovskite film (**Figure S23)**. Subsequently, we gained insights into the carrier recombination of NiO_x-based inverted PSCs without and with 3-HBA using triple cation perovskite as the absorber. **Figure S24** reveals that introducing 3-HBA can effectively reduce charge transfer resistance (R_{ct}) and increase charge recombination resistance (R_{rec}), which is attributed to the improved carrier transport, reduced defect density, and increased carrier lifetime. The improved carrier transport and transfer are also demonstrated by the transient photocurrent results (**Figure S25)**. The increased carrier lifetime from 0.242 μs to 3.81 μs shows that the nonradiative recombination is significantly reduced due to reduced defect density and boosted carrier lifetime after the passivation of 3-HBA

10.1002/anie.202206914

(**Figure 5h**). As revealed in **Figure S26**, the smaller leakage current can be observed in the 3-HBA modified device in comparison with the control device, which further indicates that the charge transfer is improved and the charge recombination loss is reduced after 3-HBA modification. As presented in **Figure 5i**, the ideality factor *n* (1.15) of the 3-HBA modified device is closer to 1 than that of the control device (1.71), indicating that the carrier non-radiative recombination is greatly reduced after modification.

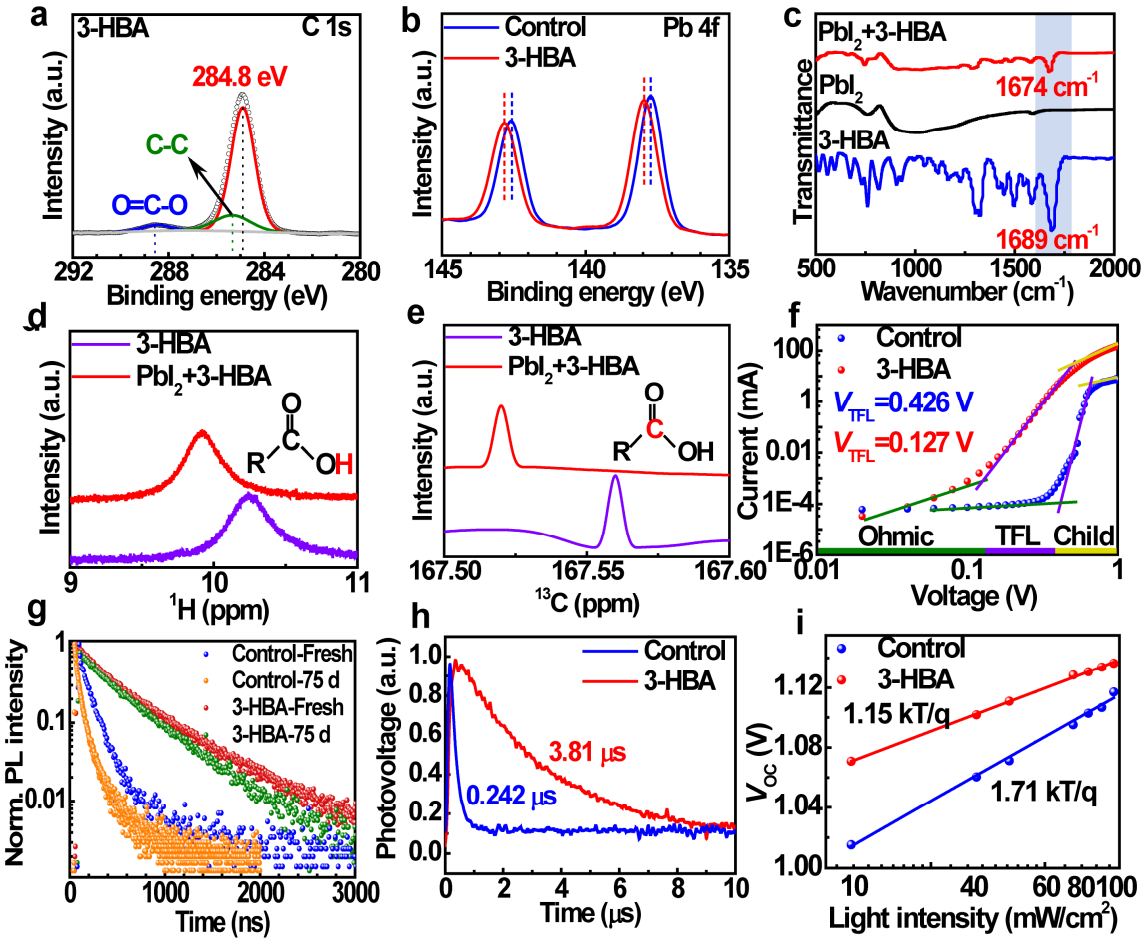

Figure 5. a) C 1s and b) Pb 4f XPS spectra of the perovskite films based on the fresh precursor solutions without and with 3-HBA. c) FTIR spectra ranging from 500 cm^{-1} to 2000 cm^{-1} of 3-HBA, PbI_2, and PbI_2+3-HBA. d) ^{1}H NMR and e) ^{13}C NMR spectra of 3-HBA and PbI_2+3-HBA solutions dissolved into DMSO-d6. f) Dark *I-V* curves of the electron-only devices (ITO/SnO_2/Perovskite/PCBM/Ag). g) TRPL spectra of the perovskite films based on the fresh and 75 d-aged precursor solutions without and with 3-HBA. h) Transient photovoltage decay curves of the control and target

inverted devices based on triple cation perovskite. i) V_{OC} as a function of light intensity for the control and 3-HBA modified inverted devices based on triple cation perovskite.

The NiO_x based inverted PSCs were fabricated and the corresponding device configuration is exhibited in **Figure 6a**. The effect of concentration of 3-HBA on device performance was compared (**Figure S27**). As exhibited in **Figure 6b** and **Table S4**, the inverted target device with triple-cation perovskite gives a PCE of 21.75% while the control device produces a PCE of 20.49%. Improved PCE is mainly a result of increased open-circuit voltage (V_{OC}) and fill factor (FF), which should be put down to the effective passivation of 3-HBA for the defects at GBs. To further increase short-circuit current density (J_{SC}), MA-free perovskite $FA_{0.95}Cs_{0.05}PbI_3$ with a narrower bandgap was utilized to fabricate inverted devices (**Figure S28**). As presented in **Figure 6c and Table S5**, the best-performing inverted target device with CsFA-based perovskite delivers a PCE of 23.49% in reverse scan (J_{SC} of 25.38 mA/cm^2, a V_{OC} of 1.138 V, and an FF of 0.814) and a PCE of 23.25% in forward scan (J_{SC} of 25.38 mA/cm^2, a V_{OC} of 1.140 V, and an FF of 0.803). To the best of our knowledge, our achieved efficiency (23.49%) is one of the highest efficiencies ever reported for NiO_x-based inverted PSCs (**Table S6**). More importantly, we achieve an attractive certified PCE of 23.33% with a J_{SC} of 25.82 mA/cm^2, a V_{OC} of 1.161 V, and an FF of 0.778 (**Figure S29-S32**). The integrated current density is well consistent with J_{SC} from *J-V* curve (**Figure S33**). We also fabricated SnO_2-based regular PSCs using nominal $FA_{0.97}Cs_{0.03}PbI_3$ perovskite films prepared by sequential deposition. The PCE is improved from 21.94% of the control device to 23.48% of the target device (**Figure S34** and **Table S7**). The above results indicate that 3-HBA is one universal defect passivator which is independent of device structure and perovskite composition. Finally, it can be concluded that 3-HBA can not only stabilize precursor solution but also improve photovoltaic performance by passivating the defects at GBs.

The stabilities of the control and 3-HBA modified films and devices were tested.

10.1002/anie.202206914

We can observe from **Figure S35** that the control film gradually turns yellow as the aging time increases while the 3-HBA-modified film remains black even if after 20 d. As can be seen from SEM images after aging for 20 d (**Figure S36**), the perovskite grains at some regions have decomposed completely and the ITO substrate is exposed whereas the target film still has a complete and flat morphology, suggesting that much more severe decomposition can be found in the control film than the target film. In addition, it can be found in **Figure S37** that just slightly reduced UV-vis absorption intensity is observed for the aged target film with respect to the fresh target film while the control film exhibits markedly decreased UV-vis absorption intensity after being aged for 20 d. As shown in **Figure S38**, the control film almost converts into the yellow phase after aging of 20 d while only a tiny amount of yellow phase is produced and the peak intensity of PbI_2 slightly increases for the target film. In one word, the above results strongly demonstrate that the moisture stability of perovskite films is much improved after modification.

As for the stability of unencapsulated PSCs, the target device can maintain 96% of its initial PCE after storing in the dark condition with a relative humidity of 10-20% for 2016 h while the control device retains only 57% after 1344 h (**Figure 6d and Figure S39**). In addition, we also performed thermal stability measurements in the dark at 85 °C in a nitrogen-filled glove box (**Figure 6e** and **Figure S40**). The target device degrades by 28% after 672 h, while the control device degrades by 45% just after 240 hours. We examined the long-term operational stability of the unsealed control and target devices by maximum power point tracking under continuous one sunlight illumination (**Figure 6f** and **Figure S41**). The PCE of the control device degrades to 65% of its original efficiency after 385 h whereas the PCE of the target device degrades to 94% of its initial efficiency after 601 h. The reduced trap-assisted nonradiative recombination due to effective defect passivation by 3-HBA should be mainly responsible for enhanced film and device stability.[8, 33, 36, 39]

10.1002/anie.202206914

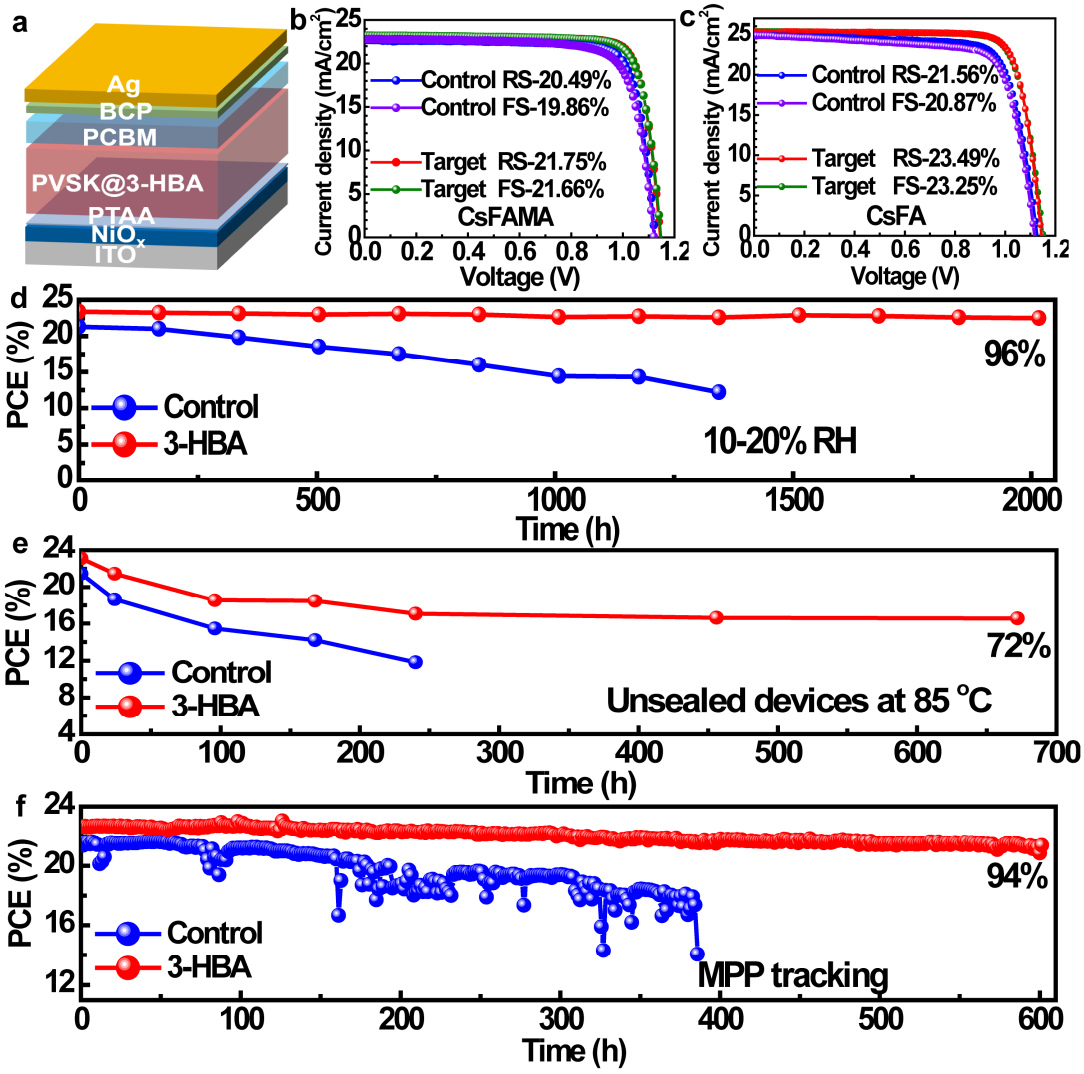

Figure 6. a) The device structure of NiO_x-based inverted PSC in this work. b) *J-V* curves of the champion inverted control and target devices based on triple-cation perovskite $Cs_{0.05}(FA_{0.83}MA_{0.17})_{0.95}Pb(I_{0.83}Br_{0.17})_3$ films. c) *J-V* curves of the champion inverted control and target devices based on MA-free perovskite $FA_{0.95}Cs_{0.05}PbI_3$ films. d) Moisture stability of the unsealed control and target devices aged under a relative humidity of 10%-20% in the dark. e) Thermal stability in the nitrogen-filled glove box at 85°C of the unsealed control and target devices aged in the dark. f) Maximum power point tracking for the control and target inverted devices based on double-cation perovskites under one sun illumination of 100 mW/cm^2 provided by white light LED in a self-made packaged test instrument full of N_2 atmosphere at 25±3 °C.

10.1002/anie.202206914

Conclusion

In summary, we have demonstrated a simple and effective precursor stabilization and defect passivation strategy where multifunctional 3-HBA containing both -COOH and -$NHNH_2$ functional groups is incorporated into perovskite precursor solution. It is uncovered that the oxidation of I^-, the deprotonation of organic cations and the following amine-cation reaction should be mainly responsible for the degradation mechanisms of mixed-organic-cation metal halide perovskite precursor solution. The -$NHNH_2$ in 3-HBA can reduce I_2 defects back to I^- and thus suppress the oxidation of I^-. At the same time, -COOH in 3-HBA as weak acid can produce hydrogen proton by reversible equilibrium ionization reaction, which can inhibit the deprotonation of organic cations and subsequent amine-cation reaction. The synergistic effect of -$NHNH_2$ and -COOH enables simultaneous suppression of the above degradation reactions. Moreover, the 3-HBA is certified to be one universal defect passivator regardless of perovskite composition and device configuration. As a result, the resulting NiO_x-based inverted device produces an attractive efficiency of 23.5% (certified PCE of 23.33%). The modified devices with 3-HBA maintain 94% of the initial efficiency after maximum power point tracking under continuous illumination for 601 hours. The precursor solution stabilization and defect passivation strategy developed in this work will contribute to accelerating the industrialization of perovskite optoelectronic devices.

Acknowledgments

This work was supported by the National Natural Science Foundation of China (Grant Nos. 62004058, U21A2076, 52071048), Nature Science Foundation of Hebei Province (F2020202022), the Open Fund of the State Key Laboratory of Integrated Optoelectronics (IOSKL2020KF09), State Key Laboratory of Reliability and Intelligence of Electrical Equipment (No. EERI_PI20200005, EERI_0Y2021001), The Central Guidance on Local Science and Technology Development Fund of Hebei Province(Grant No. 226Z4305G). This work was also supported by Support plan for

Overseas Students to Return to China for Entrepreneurship and Innovation (Grant No. cx2020003), the Fundamental Research Funds for the Central Universities (Grant No. 2020CDJ-LHZZ-074), and Natural Science Foundation of Chongqing (Grant No. cstc2020jcyj-msxmX0629).

Conflict of Interest

The authors declare no conflict of interest.

References

[1] J. Jeong, M. Kim, J. Seo, H. Lu, P. Ahlawat, A. Mishra, Y. Yang, M. A. Hope, F. T. Eickemeyer, M. Kim, *Nature* **2021**, *592*, 381.

[2] X. Li, W. Zhang, X. Guo, C. Lu, J. Wei, J. Fang, *Science* **2022**, *375*, 434.

[3] H. Min, D. Y. Lee, J. Kim, G. Kim, K. S. Lee, J. Kim, M. J. Paik, Y. K. Kim, K. S. Kim, M. G. Kim, *Nature* **2021**, *598*, 444.

[4] R. Azmi, E. Ugur, A. Seitkhan, F. Aljamaan, A. S. Subbiah, J. Liu, G. T. Harrison, M. I. Nugraha, M. K. Eswaran, M. Babics, *Science* **2022**, eabm5784.

[5] Q. Chen, J. Chen, Z. Yang, J. Xu, L. Xu, C. Liang, X. Han, Z. Liu, *Adv. Mater.* **2019**, *31*, 1802228.

[6] J. J. Yoo, G. Seo, M. R. Chua, T. G. Park, Y. Lu, F. Rotermund, Y.-K. Kim, C. S. Moon, N. J. Jeon, J.-P. Correa-Baena, *Nature* **2021**, *590*, 587.

[7] https://www.nrel.gov/pv/assets/pdfs/best-research-cell-efficiencies-rev211214.pdf.

[8] L. Zhu, X. Zhang, M. Li, X. Shang, K. Lei, B. Zhang, C. Chen, S. Zheng, H. Song, J. Chen, *Adv. Energy Mater.* **2021**, *11*, 2100529.

[9] X. Wang, Y. Fan, L. Wang, C. Chen, Z. Li, R. Liu, H. Meng, Z. Shao, X. Du, H. Zhang, G. Cui, S. Pang, *Chem* **2020**, *6*, 1369.

[10] S. Wang, Y. Li, J. Yang, T. Wang, B. Yang, Q. Cao, X. Pu, L. Etgar, J. Han, J. Zhao, X. Li, A. Hagfeldt, *Angew. Chem. Int. Ed.* **2022**, *61*, e202116534.

[11] J. Kim, B.-w. Park, J. Baek, J. S. Yun, H.-W. Kwon, J. Seidel, H. Min, S. Coelho, S. Lim, S. Huang, K. Gaus, M. A. Green, T. J. Shin, A. W. Y. Ho-baillie, M. G. Kim, S. I. Seok, *J. Am. Chem. Soc.* **2020**, *142*, 6251.

[12] M. Ozaki, A. Shimazaki, M. Jung, Y. Nakaike, N. Maruyama, S. Yakumaru, A. I. Rafieh, T. Sasamori, N. Tokitoh, P. Ekanayake, *Angew. Chem. Int. Ed.* **2019**, *58*, 9389.

[13] G. S. Shin, S. G. Kim, Y. Zhang, N. G. Park, *Small Methods* **2020**, *4*, 1900398.

[14] D. P. McMeekin, Z. Wang, W. Rehman, F. Pulvirenti, J. B. Patel, N. K. Noel, M. B. Johnston, S. R. Marder, L. M. Herz, H. J. Snaith, *Adv. Mater.* **2017**, *29*, 1607039.

[15] Q. Dong, W. Shang, X. Yu, Y. Yin, C. Jiang, Y. Feng, J. Bian, B. Song, S. Jin, Y. Zhou, L. Wang, Y. Shi, *ACS Energy Lett.* **2022**, *7*, 481.

[16]N. K. Noel, M. Congiu, A. J. Ramadan, S. Fearn, D. P. McMeekin, J. B. Patel, M. B. Johnston, B. Wenger, H. J. Snaith, *Joule* **2017**, *1*, 328.

[17] B. Dou, L. M. Wheeler, J. A. Christians, D. T. Moore, S. P. Harvey, J. J. Berry, F. S. Barnes, S. E. Shaheen, M. F. A. M. van Hest, *ACS Energy Lett.* **2018**, *3*, 979.

[18] V. Valenzano, A. Cesari, F. Balzano, A. Milella, F. Fracassi, A. Listorti, G. Gigli, A. Rizzo, G. Uccello-Barretta, S. Colella, *Cell Rep. Phys. Sci.* **2021**, *2*, 100432.

[19] H. Tsai, W. Nie, Y. H. Lin, J. C. Blancon, S. Tretiak, J. Even, G. Gupta, P. M. Ajayan, A. D. Mohite, *Adv. Energy Mater.* **2017**, *7*, 1602159.

[20] L. Wang, H. Zhou, J. Hu, B. Huang, M. Sun, B. Dong, G. Zheng, Y. Huang, Y. Chen, L. Li, Z. Xu, N. Li, Z. Liu, Q. Chen, L.-D. Sun, C.-H. Yan, *Science* **2019**, *363*, 265.

[21] M. Li, D. Gao, B. Zhang, S. Xu, X. Zhuang, C. Wang, L. Yang, X. Ma, S. Zheng, H. Song, J. Chen, C. Chen, *Sol. RRL* **2021**, *5*, 2100320.

[22] J. Chen, D. He, N.-G. Park, *Sol. RRL* **2022**, *6*, 2100767.

[23] W. Hui, L. Chao, H. Lu, F. Xia, Q. Wei, Z. Su, T. Niu, L. Tao, B. Du, D. Li, *Science* **2021**, *371*, 1359.

[24] H. Lu, Y. Liu, P. Ahlawat, A. Mishra, W. R. Tress, F. T. Eickemeyer, Y. Yang, F. Fu, Z. Wang, C. E. Avalos, *Science* **2020**, *370*, eabb8985.

[25] M. Qin, J. Cao, T. Zhang, J. Mai, T. K. Lau, S. Zhou, Y. Zhou, J. Wang, Y. J. Hsu, N. Zhao, *Adv. Energy Mater.* **2018**, *8*, 1703399.

[26] H. Min, G. Kim, M. J. Paik, S. Lee, W. S. Yang, M. Jung, S. I. Seok, *Adv. Energy Mater.* **2019**, *9*, 1803476.

[27] C. Chen, Y. Rao, Z. Li, X. Wang, G. Cui, W. Wang, S. Pang, *Sol. RRL* **2021**, *5*, 2000715.

[28] Q. Dong, W. Shang, X. Yu, Y. Yin, C. Jiang, Y. Feng, J. Bian, B. Song, S. Jin, Y. Zhou, *ACS Energy Lett.* **2021**, *7*, 481.

[29] R. Azmi, E. Ugur, A. Seitkhan, F. Aljamaan, A. S. Subbiah, J. Liu, G. T. Harrison, M. I. Nugraha, M. K. Eswaran, M. Babics, Y. Chen, F. Xu, T. G. Allen, A. u. Rehman, C.-L. Wang, T. D. Anthopoulos, U. Schwingenschlögl, M. D. Bastiani, E. Aydin, S. D. Wolf, *Science* **2022**, *376*, 73.

[30] Z. Li, B. Li, X. Wu, S. A. Sheppard, S. Zhang, D. Gao, N. J. Long, Z. Zhu, *Science* **2022**, *376*, 416.

[31] K. Wang, C. Wu, Y. Hou, D. Yang, T. Ye, J. Yoon, M. Sanghadasa, S. Priya, *Energy Environ. Sci.* **2020**, *13*, 3412.

[32] H. Chen, S. Teale, B. Chen, Y. Hou, L. Grater, T. Zhu, K. Bertens, S. M. Park, H. R. Atapattu, Y. Gao, M. Wei, A. K. Johnston, Q. Zhou, K. Xu, D. Yu, C. Han, T. Cui, E. H. Jung, C. Zhou, W. Zhou, A. H. Proppe, S. Hoogland, F. Laquai, T. Filleter, K. R. Graham, Z. Ning, E. H. Sargent, *Nat. Photonics* **2022**, *16*, 352.

[33] J. Chen, N.-G. Park, *Adv. Mater.* **2019**, *31*, 1803019.

[34] J. Chen, N.-G. Park, *ACS Energy Lett.* **2020**, *5*, 2742.

[35] W. Zhang, S. Pathak, N. Sakai, T. Stergiopoulos, P. K. Nayak, N. K. Noel, A. A. Haghighirad, V. M. Burlakov, D. W. deQuilettes, A. Sadhanala, W. Li, L. Wang, D. S. Ginger, R. H. Friend, H. J. Snaith, *Nat. Commun.* **2015**, *6*, 10030.

[36] B. Liu, H. Bi, D. He, L. Bai, W. Wang, H. Yuan, Q. Song, P. Su, Z. Zang, T. Zhou, J. Chen, *ACS Energy Lett.* **2021**, *6*, 2526.

[37] X. Wang, X. Ran, X. Liu, H. Gu, S. Zuo, W. Hui, H. Lu, B. Sun, X. Gao, J. Zhang, *Angew. Chem. Int. Ed.* **2020**, *59*, 13354.

[38] R. Xia, X. X. Gao, Y. Zhang, N. Drigo, V. I. Queloz, F. F. Tirani, R. Scopelliti, Z. Huang, X. Fang, S. Kinge, *Adv. Mater.* **2020**, *32*, 2003801.

10.1002/anie.202206914

[39] L. K. Ono, S. Liu, Y. Qi, *Angew. Chem. Int. Ed.* **2020**, *59*, 6676.

10.1002/anie.202206914

Graphical Abstract

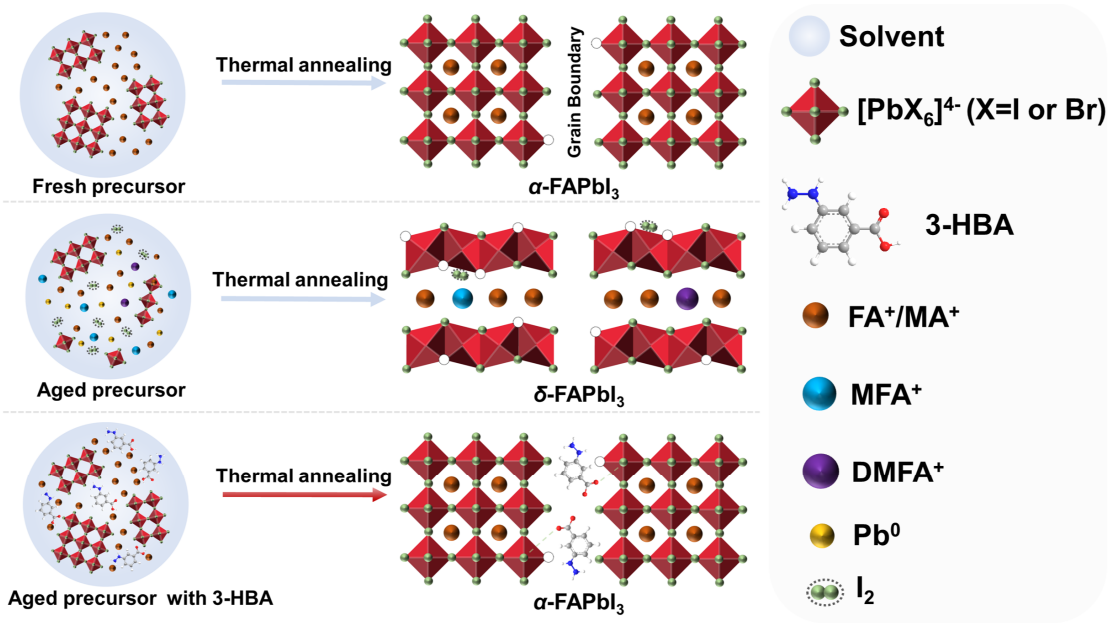

We develop a precursor stabilization and defect passivation strategy by employing 3-hydrazinobenzoic acid (3-HBA) as a versatile additive. The synergistic effect of -$NHNH_2$ and -COOH suppresses oxidation of I^-, deprotonation of organic cations and amine-cation reaction. The NiO_x-based inverted device achieves a certified efficiency of 23.3% with excellent operational stability.